Journal of Power Sources 196 (2011) 6609–6621

Contents lists available at ScienceDirect

Journal of Power Sources

journal homepage: www.elsevier.com/locate/jpowsour

Synthesis conditions, light intensity and temperature effect on the performance of ZnO nanorods-based dye sensitized solar cells

Irene Gonzalez-Valls[a], Youhai Yu[a], Belén Ballesteros[a,1], Judith Oro[b], Monica Lira-Cantu[a,*]

[a] Centre d'Investigació en Nanociència i Nanotecnologia (CIN2, CSIC-ICN), Campus UAB, Edifici ETSE 2nd Floor. Bellaterra (Barcelona) E-08193, Spain[1]
[b] Institut de Ciencia de Materials de Barcelona (ICMAB, CSIC), Campus UAB, Bellaterra (Barcelona) E-08193, Spain

ARTICLE INFO

Article history:
Received 4 January 2011
Received in revised form 22 February 2011
Accepted 27 March 2011
Available online 6 April 2011

Keywords:
ZnO nanorods
Dye-sensitized solar cells
Temperature effect
Light intensity effect
UV light effect
Stability analysis
Hybrid solar cells

ABSTRACT

We present in this work a careful study of the different parameters affecting vertically-aligned ZnO-nanorods (NRs) based dye sensitized solar cells (DSCs). We analyze the effect of synthesis conditions, light intensity, UV light and working temperature, and correlated them to the final photovoltaic properties of the DSC. Although similar studies can be found in the literature for DSCs based on TiO_2, this work is, to our knowledge, the first detailed study carried out for DSC based on vertically-aligned ZnO nanorods. The ZnO NRs were grown between 1.6 and 5.2 μm long. Electrodes made with 1.6 ± 0.2 μm thickness were used to analyze parameters such as synthesis conditions, light intensity (800–1500 W m^{-2}), UV light irradiation and temperature (25–75 °C). We have also carried out initial analysis of the solar cell lifetime under continuous light irradiation at 45 °C, and analyzed the ZnO electrode before and after testing. The best photovoltaic response was characterized by a power conversion efficiency of 1.02%, with J_{sc} of 3.72 mA cm^{-2}, V_{oc} of 0.603 V and 45% FF (at 72 °C), for a ZnO NR electrode of 5.2 μm thickness. Comparison of our power conversion efficiency values with published data is also presented, as well as a brief discussion on the possible reasons behind the low power conversion efficiency observed for these type of solar cells.

1. Introduction

The application of ZnO in photovoltaics is not limited to act as electron transport material (ETM) in dye sensitized solar cells (DSC) and hybrid solar cells (HSC) [1]. It can also be find applied as antireflection coating in inorganic solar cells [2,3], or as optical spacer in polymer solar cells (tandem, hybrid and inverted organic solar cells) [4–7]. The true consciousness about the potential impact of ZnO emerged once the simplicity of its synthesis was revealed, together with its availability and low cost. The possibility to obtain ZnO in a broad variety of nanostructures, on almost all types of substrates and at low temperatures, opened up the opportunity for its application in a wide variety of devices: solar cells, light emitting diodes, field effect transistors, electrochemical sensors, piezoelectric and thermoelectric devices, etc. Thus, there is a great need to study and understand how different parameters affect ZnO-based devices. Interest on ZnO-based dye sensitized solar cells (DSCs) has been sturdily increased since power conversion efficiency rose up to 6.1% in 2010 applying ZnO nanoparticles [8]. Nanostructures of ZnO can be found as simple nanoparticles or as nanorods, nanobelts, branched nanorods, nanowires, ultranarrow nanobelts, hierarchical nanostructures, nanocombs, nanosprings, nanospirals, searnless nanorings, core–shell nanostructures, nanocages, nanoflowers, among many others [1,9,10]. The synthesis of one-dimensional (1D) nanostructures for solar cells has been recently reviewed for semiconductor oxides in general [11] and for ZnO nanostructures in particular [1,12,13]. In DSC applying vertically-aligned ZnO NRs, the main problem is their low surface area, nanorods between 20 and 25 μm have shown only 1/5 of the surface area of a similar electrode made of nanoparticles. The latter seems to be the main reason why reported power conversion efficiencies applying bare vertically aligned ZnO nanorods have not been higher than 2.5%, not even when NRs with lengths up to 40 μm are applied [14]. Yet, enormous efforts are being invested in order to understand these causes and to find new ways to improve ZnO properties. In this work, we present our most recent study carried out on dye sensitized solar cells based on vertically-aligned ZnO nanorods. We have analyzed different parameters for the synthesis conditions that affect final ZnO nanorod formation. We also analyzed the effect on photovoltaic performance depending on temperature, light irradiation or the application of UV light. Although similar studies can be found in the literature for TiO_2 based DSCs, this work is to our knowledge, the first detailed study carried out for DSC based on ZnO nanorods. Our goal is to analyze the behaviour of these types of solar cells under real (simulated out-

* Corresponding author. Tel.: +34 93 586 8011; fax: +34 93 586 8020.
E-mail address: monica.lira@cin2.es (M. Lira-Cantu).
[1] http://www.cin2.es.

0378-7753/$ – see front matter © 2011 Elsevier B.V. All rights reserved.
doi:10.1016/j.jpowsour.2011.03.063

door) conditions. We finally compare our results with DSC applying vertically-aligned nanostructures of ZnO with published works and discuss the possible causes for the ZnO-based DSC limited efficiency.

2. Experimental

2.1. Materials

All chemicals were commercial materials and used without further purification: methanol (99.8% Aldrich), ethanol (99.5% Panreac) zinc acetate dehydrate (99% Riedel-de Haën), KOH (Na <0.002% Fluka), hexamethylenetetramine (HMT) (99% Aldrich), zinc nitrate hexahydrate ($Zn(NO_3)_2{\cdot}6H_2O$) (98% Sigma–Aldrich), diethanolamine (≥98% Sigma–Aldrich). Indium-tin oxide (ITO) or Fluor-tin oxide (FTO) slides were purchased from Solems and they were cleaned by standard procedures prior to use. Iodolyte AN-50 (50 mM tri-iodide in acetonitrile), dye $(Bu_4N)_2Ru(debpyH)_2(NCS)$ (Ruthenium 535-bisTBA also known as N-719), Pt-paste Pt-catalyst T/SP and hot melt sealing foil (SX1170) were from Solaronix. All the aqueous solutions were prepared using double distilled and ion-exchange water.

2.2. Preparation and characterization of ZnO nanorods (NRs) films

The growth of the vertically-aligned ZnO NRs can be made on two transparent conducting oxides (TCO), indium tin oxide (ITO), or fluor tin oxide (FTO) without affecting the final NR dimensions or properties. Nevertheless, since ITO conductivity is well known to be susceptible to temperatures above 450 °C, the analyses (on temperature, UV light and light intensity) performed on the final solar cells were carried out applying FTO substrates. For the synthesis of the nanorods, the TCO substrates were first washed with milli-Q water, ethanol and acetone, dried under N_2 flux and cleaned for 20 min in a UV-surface decontamination system (Novascan, PSD-UV) connected to an O_2 gas source before use. A ZnO buffer layer of about 80–100 nm thick was prepared by spin coating a sol–gel layer of ZnO on top of the TCO substrate. The ZnO sol–gel was prepared using the method previously reported [15,16]. Briefly, 2.0 g of zinc acetate and 1.07 g of diethanol amine (DEA) were dissolved in 10 mL of isopropanol and heated at 60 °C for about 10 min until total dissolution, then the solution was diluted with ethanol (1:1) and filtered through a 0.45 μm pore (Albet). Once the ZnO by sol–gel was applied by spin coating, the substrates were annealed at 450 °C for 2 h (heating ramp 3 °C min^{-1}). The latter procedure allows for the formation dense ZnO thin film used as buffer layer which permits a better contact between the TCO and ZnO nanorods (NRs). A layer of ZnO nanoparticles (NPs), used as seeds for the growth of the ZnO nanorods (NRs), was spin coated on top of the ZnO buffer layer. The ZnO nanoparticles were prepared following the method described by Pacholski et al. [17]: a solution of 0.03 M KOH in methanol was added dropwise in a refluxing mixture of zinc acetate dehydrate 0.01 M in methanol at 65 °C. After 2 h of reflux the solution was allowed to cool down. Since the suspension of the ZnO nanoparticles is known to degrade (agglomerate) with time [21], we use always a freshly prepared suspension. The suspension of the nanoparticles was spin coated on the ITO/ZnO dense layer for 3 times at a speed of 1000 rpm [18]. Thermal treatments were made to the substrates at 150 °C for 10 min between each deposition was made. To grow the ZnO NRs, the substrates were placed face-down in an equimolar aqueous solution of 25 mM zinc nitrate hexahydrate and HMT [19,20,22] at 96 °C between 1 h and 22 h, changing the solution every 4–6 h. Since thermal treatment to the as-synthesized electrodes is known to improve power conversion efficiency, the samples were dried in air and sintered at 450 °C for 30 min in air before DSC fabrication. Characterization of the ZnO nanoparticles and nanorods was carried out in a scanning electron microscopy (SEM, HITACHI-S-570), transmission electron microscopy (TEM, 120 kV – JEOL 1210 equipped with EDS analyzer LINK QX 2000 X and JEOL 2011 operated at 200 kV). X-ray powder diffraction analyses between 5 and 120° were carried out in a XRD, RIGAKU Rotaflex RU200 B instrument, using Cu$K\alpha_1$ radiation. UV–visible analyses of solutions and thin films were made in a Shimadzu 1800.

2.3. Solar Cell fabrication and characterization

NRs arrays on the TCO substrate were first sensitized in a 0.5 mmol L^{-1} solution of $(Bu_4N)_2Ru(debpyH)_2(NCS)$, (N-719 dye) at different times between 10 and 960 min, at room temperature, 60 °C and 100 °C. Platinized FTO counter electrode, prepared by doctor blade using a Pt-paste Catalyst T/SP and annealed at 450 °C for 30 min, was then bounded thermally together with the NRs electrode using a hot melt sealing foil. A liquid electrode was used to fill the internal space between electrodes by capillary forces. For the temperature and light intensity studies, the cells were sealed with Surlyn (Solaronix) using vacuum. The solar simulation was carried out with a Steuernagel Solarkonstant KHS1200 equipped with an AM1.5 filter for all characterization (1000 W m^{-2}, AM1.5G, 72 °C). The calibration was made according to ASTM G173. IV-curves were measured using a Keithley 2601 multimeter. Light intensity was 1000 W m^{-2} calibrated, a Zipp & Konen CM-4 pyranometer is used constantly during measurements to set light intensity and a calibrated S1227-1010BQ photodiode from Hamamatsu is also applied for calibration before each measurement. IPCE analyses were carried out with a QE/IPCE measurement System from Oriel at 10 nm intervals between 300 and 700 nm. The results were not corrected for intensity losses due to light absorption and reflection by the glass support. For the experiments where the light intensity, the UV filter and the temperature were studied, we applied DSCs with vertically-aligned ZnO NR of ~1.8 μm in length (grown for 6 h). The electrodes were immersed in the dye solution for 2 h and the solar cell was completed by sealing a Pt counter electrode with the hot-melt sealing. Finally the device was filled with the electrolyte. Solar cells were then introduced to a home-made cell holder with temperature and gas control. Measurements were carried out between 25 °C and 75 °C. At the same time the incident power light was varied between 800 and 1500 W m^{-2}. The experiments were also carried out with and without a UV-light; the UV light was blocked by placing an UV filter (Thorlabs FS400, <400 nm) on top of the quartz-crystal window. Before measurements, cells were allowed to stabilize at the desired temperature for 10 min and for 5 min more at each incident light. All the DSCs were carefully sealed to avoid electrolyte losses and device degradation. The home-made solar cell holder used in these studies is described in Ref. [65]. It is a two-piece glass reactor with a cooling jacket for temperature control, with a home-designed o-ring sealed cap. It has ports for thermocouple, inlet and outlets for low pressure gas flow, quartz window (5 cm diameter) and cable connections. An UV filter can be placed on top of the quartz window. The holder can analyze up to two 1 cm by 2.5 cm solar cells, but larger reactors, with 15 cm diameter quartz window, can hold larger solar cells [65]. The temperature of the experiments was monitored with a digital thermohygrometer (HD2301/01, Afora).

3. Results and discussion

This section describes the different factors that must be consider in order to obtain reproducible electrodes made of vertically-aligned ZnO NRs. We then present the application of these

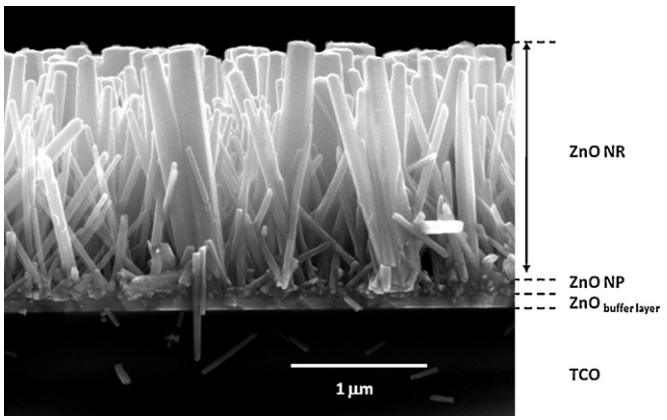

Fig. 1. A representative lateral view of a ITO/ZnO buffer layer/ZnO NRs electrode. The ZnO buffer layer of 80 nm thickness, is made by sol-gel synthesis by spin coating. A layer of nanoparticles (NP) is used as seeds for the nanorod (NRs) growth.

electrodes as part of DSCs and analyze most of the issues that can modify solar cell performance (light irradiation, temperature, etc.). We finally compare our results with already published work and discuss on the possible reason for the low solar cell performance find with ZnO based DSC.

3.1. Effect of synthesis conditions

The vertically-aligned NRs are usually obtained on an ITO substrate applying a dense thin film of ZnO used as buffer layer (about 80 nm [24]). A layer of ZnO nanoparticles (NPs) is then deposited by spin coating. The nanoparticles are used as seeds to grow the ZnO NRs, which length depend on the growth time and can vary between a few nanometers up to 5 μm. A representative image of a lateral view of the ITO/ZnO_{dense}/ZnO NRs grown for 6 h is shown in Fig. 1. For the fabrication of a complete DSC an electrode (as shown in Fig. 1) is sandwiched together with a Pt electrode and an electrolyte is filled between both electrodes.

3.1.1. Seeds of ZnO NP

In order to cope with the electron diffusion length, the synthesis of ZnO NRs must be obtained with small NR diameters (about 20–50 nm). The latter depends on many factors, especially on the diameter of the ZnO NPs used as seeds for NR growth. During the synthesis of the ZnO nanoparticles, a white-cloudy solution develops with time. To control NPs size and agglomeration, the cloudy suspension was analyzed by TEM at different periods of time. Fig. 2 shows TEM images of the nanoparticles obtained. It can be observed that at early stages of the synthesis, the NPs have a size between 5 and 7 nm (Fig. 2a) and grow slowly until reaching a homogeneous size of 10–12 nm after 2 h of reflux (Fig. 2b). The agglomeration of the NPs within the solution was observed 4 h after synthesis at room temperature (Fig. 2c), a behaviour also observed by Ali and Winterer [21]. Thus, the synthesis of vertically-aligned ZnO NRs was always carried out applying freshly-prepared NPs.

3.1.2. NR growth and the concentration of reactants

For the synthesis of the NRs many parameters were studied. A remarkable effect on NR dimensions, especially NRs diameter, was observed with the modification of the distance between the ITO/ZnO substrate and the bottom of the reaction flask [1]. Fig. 3 shows ZnO NRs grown at different distances between the flask's bottom and the ITO substrate: at 1 cm (Fig. 3a) and at 7 cm (Fig. 3b). We observed that substrates placed closer to the bottom of the reaction flasks initiate nanoparticles nucleation earlier. Moreover, the growth of the NRs was observed to initiate faster for substrates at 1 cm distance (Fig. 3a) than the substrates placed at 7 cm distance (Fig. 3b). Most important is that the smallest diameters (ideal for solar cell application) were found when the substrates were placed far away from the bottom of the flask (Fig. 3c and d). Since we need small ZnO NRs diameters in order to cope with the electron diffusion length required in excitonic solar cells, ~20 nm [1], distances between 6 and 8 cm between substrate and the bottom of the reaction flask were chosen. Another important factor is the concentration of the reaction solution. We use a 25 mM equimolar solution of the reactants since increasing the solution concentration above 25 mM, resulted in the formation of NRs with larger diameters, also less packing density of the ZnO nanorods covering the electrode area (Fig. 3e and f) was observed.

3.1.3. Growth time

Optimization of the NR dimensions, length and diameter, was carried out by modifying the growth time. We synthesized the NRs at different growth times, between 1 h and 22 h, the hydrothermal solution was changed every 6 h. As it was expected, the length of NRs increases with growth time, achieving NRs lengths as long as 5.2 μm at 22 h, as shown in Fig. 4. The majority

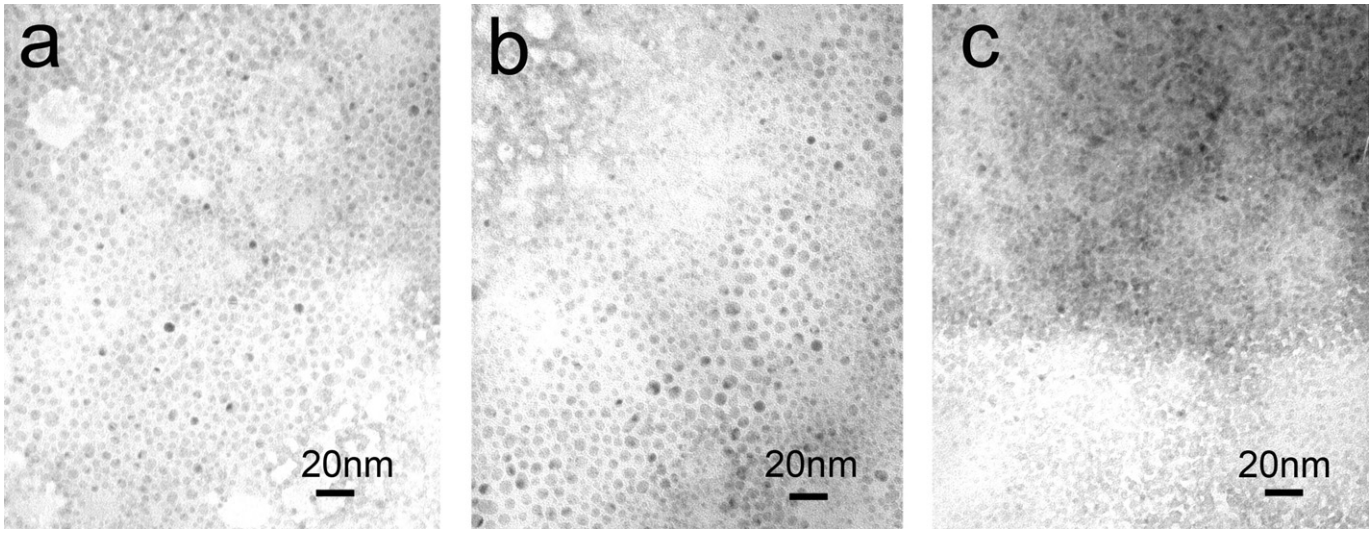

Fig. 2. TEM images of the ZnO NPs solution at different points during and after the synthesis: (a) at 30 min of reflux, (b) at 2 h of reflux and (c) at 4 h after the synthesis was finished.

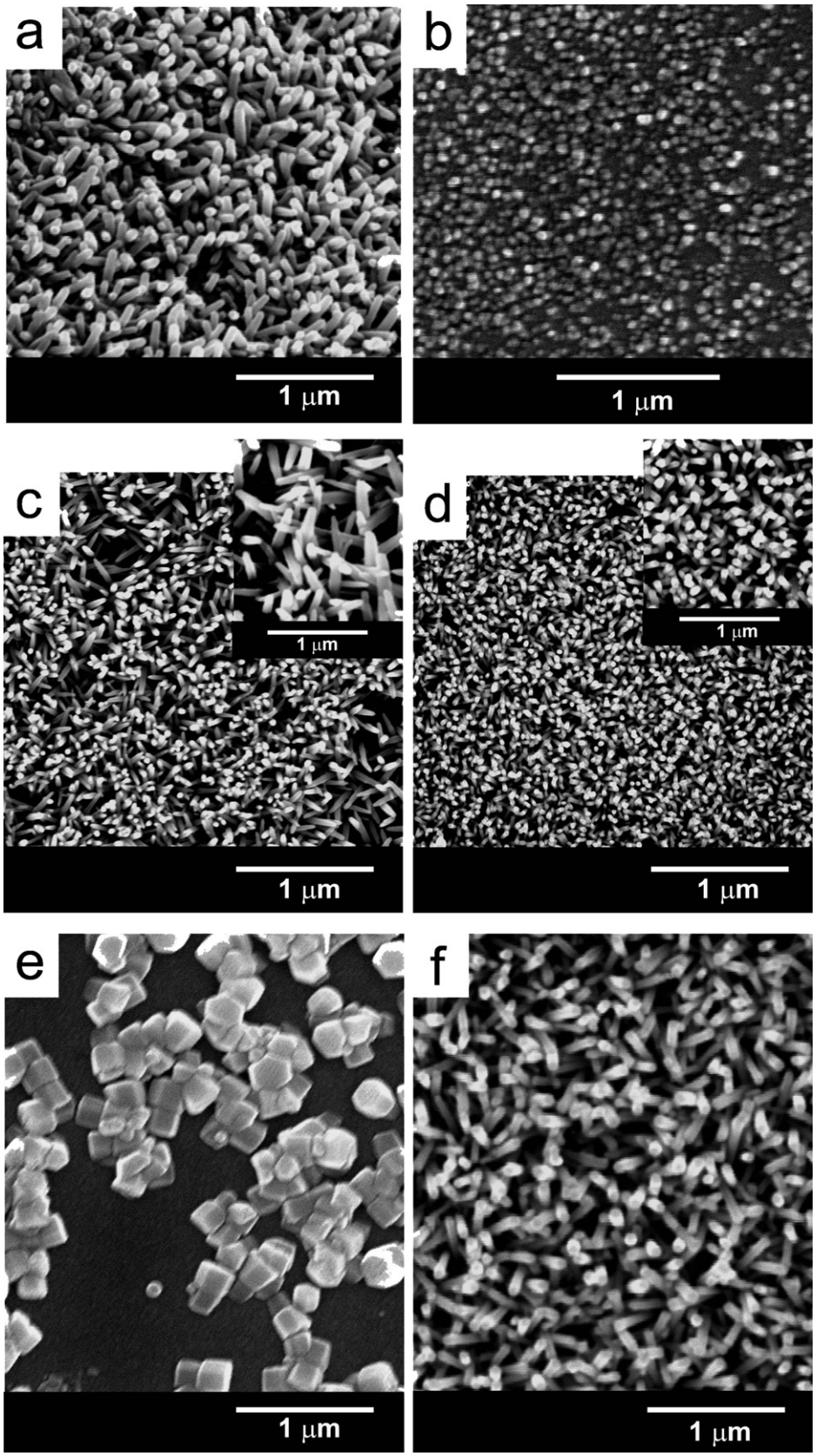

Fig. 3. SEM images of vertically-aligned ZnO NRs. (I) Effect of the distance between the substrate and the bottom of the reaction flask at 30 min growth time: (a) 1 cm and (b) 7 cm. (II) Effect of the distance between the substrate and the reaction flask after 2 h growth, NR diameters: (c) 150 nm NR diameter for a 1 cm distance and (d) 40 nm NR diameter for a 7 cm distance. (III) Effect of the concentration of the reactants on ZnO grown for 1.5 h growth time: (e) 0.1 M and (f) 0.025 M.

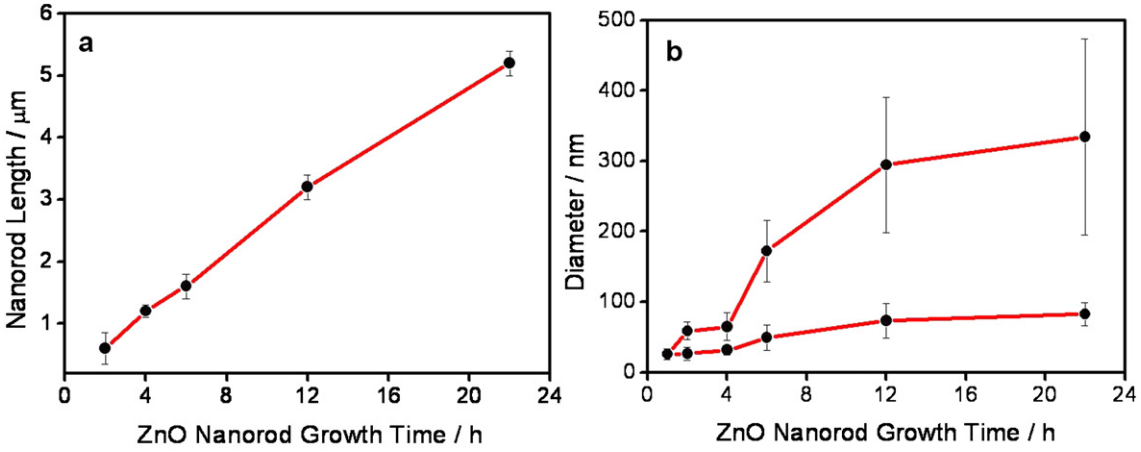

Fig. 4. Variation of vertically aligned ZnO NRs dimensions with growth time (a) length and (b) diameter.

of diameters were found to be around 40 nm, although a few NRs presented larger diameters (Fig. 4b). We also observed that longer growth times resulted in the presence of large amounts of broken NRs attached to the surface (some of them with huge dimensions), this can be avoided by the use of additives [23]. Nevertheless, the application of additives is beyond the scope of this manuscript.

3.1.4. NRs characterization

Fig. 5 shows SEM images of vertically-aligned ZnO NRs grown at 12 h and 22 h (NRs grown for 2 h, 4 h and 6 h have been previously reported [24]), the cross section view is shown in Fig. 5a and b respectively, and top view in Fig. 5c and d respectively. Top view of the electrodes shows the majority of the ZnO NR diameters being about 40 nm with the presence of a few NRs with longer diameter.

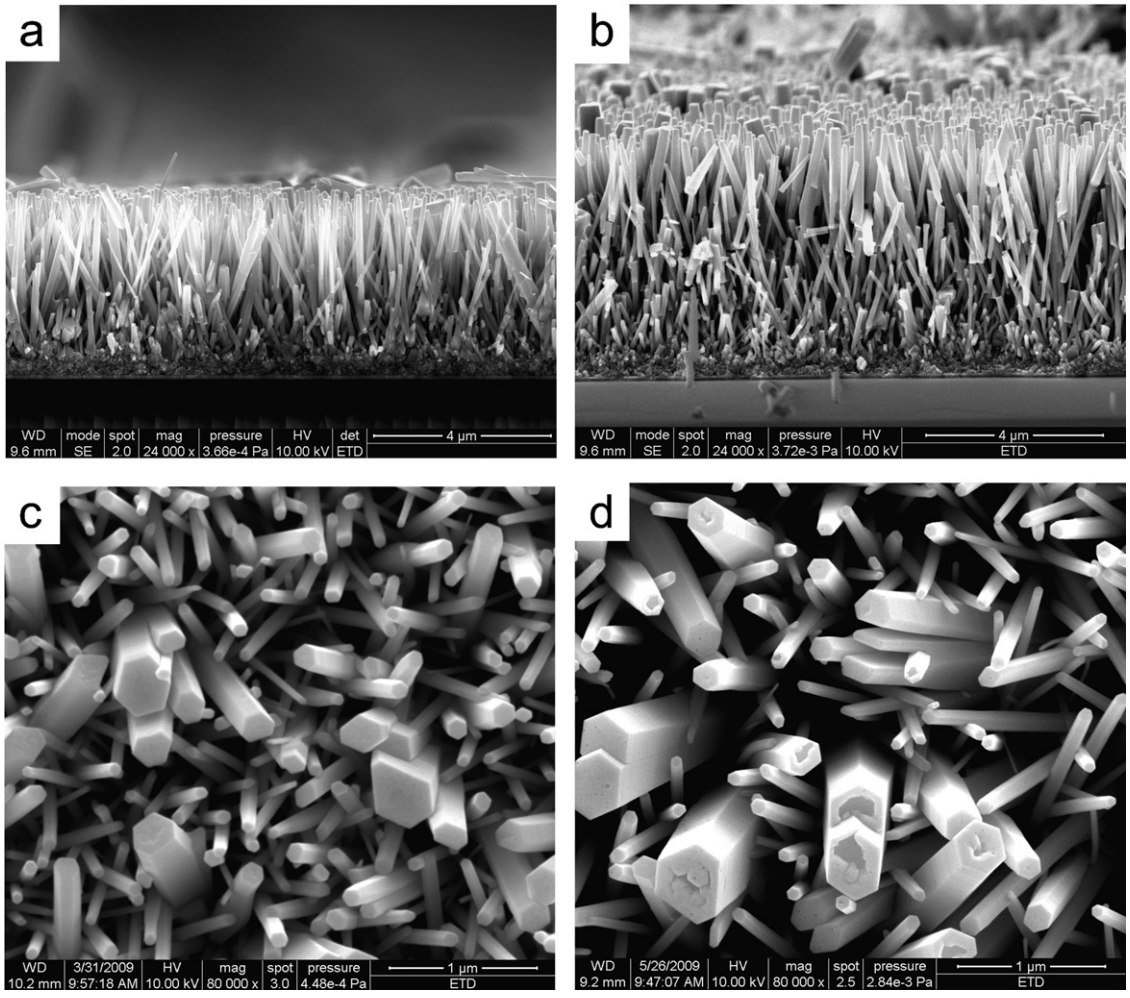

Fig. 5. FE-SEM Images of ZnO NR electrodes grown at 12 h (a, c) and 22 h (b, d). Cross-section view: inclination at 90° (a, b); and top view (c, d).

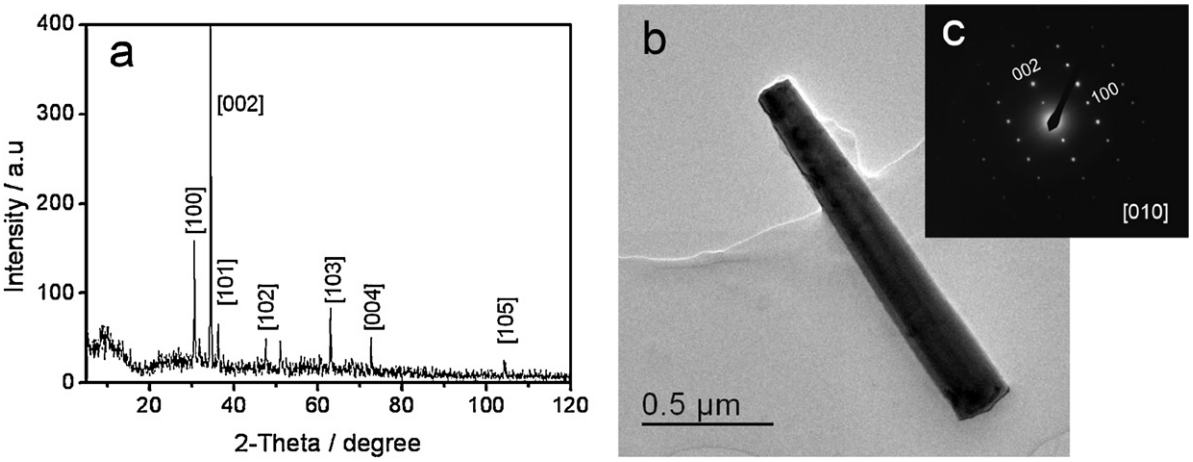

Fig. 6. (a) XRD pattern of ZnO nanorods grown on ITO. (b) TEM image of a single ZnO NR of 6 h growth time and (c) Selected-area electron diffraction (SAED) pattern of the ZnO NR.

Characterization of the ZnO electrodes by X-ray diffraction showed the presence of ZnO in its wurtzite phase and the peak [0 0 2] indicates preferential orientation due to the vertical growth of the NRs on the ITO substrate (Fig. 6a). TEM analyses of scratched NRs from the surface of the electrode confirmed good crystallinity (Fig. 6b and c).

As a summary of this section, we have shown how all the parameter for the synthesis of the ZnO NRs must be carefully controlled. In our case, reproducible electrodes of vertically-aligned ZnO NRs were grown when an 80 nm dense layer of ZnO was used as buffer layer, and a layer of ZnO NPs was deposited afterwards. The NPs were used as seeds and were applied before 4 h after their synthesis to avoid NP agglomeration. The best results with respect to NRs dimensions were found at about 7 cm distance between the substrate and the bottom of the reaction flask.

3.2. Application of ZnO nanorods in dye-sensitized solar cells

The vertically-aligned ZnO NRs were used as front electrodes in DSC applying a Pt as the back electrode. Our initial results show that the DSC performance improved after sintering the ZnO NRs electrodes at 450 °C for 30 min as shown in Fig. 7a. Power conversion efficiency was observed to increase from 0.48% up to 0.62%, V_{oc} registered slight changes from 0.45 to 0.5 V and J_{sc} improved from 3.1 mA cm^{-2} to 3.7 mA cm^{-2} (for ZnO NRs of ~2 μm length). Improvement after thermal treatment is related to the presence of defects, e.g. oxygen vacancies [25], usually observed in amorphous oxides [26]. These oxygen vacancies (or deep donor states) act as traps for electrons [27] and thus, as recombination centers [28]. The clear consequence of electron–hole recombination is the reduction of the power conversion efficiency of the device [29]. Thus, the incorporation of oxygen during thermal treatment is well-known to modify optical properties of semiconductor oxides affecting photovoltaic properties. The optical band gap of these materials is very sensitive to oxygen incorporation, which in turn, could be the responsible for the increase observed for V_{oc} [30–32]. Our electrodes were then systematically treated in air at 450 °C before analysis as electrode in DSC.

We carried out the optimization of the dye sensitization of the ZnO electrodes with the Ru(II) complex dye, $(Bu_4N)_2(debpyH)_2(NCS)$, also known as N-719. The best dye loading time (DLT) found for ZnO NR with lengths of ~0.6 μm, ~1.1 μm, ~1.6 μm, ~3.2 μm and ~5.2 μm were found to be 10 min, 2 h, 2 h, 3 h, and 6 h, respectively. Longer dye loading times for each ZnO NR length resulted in reduced solar cell efficiency due to dye agglomeration.

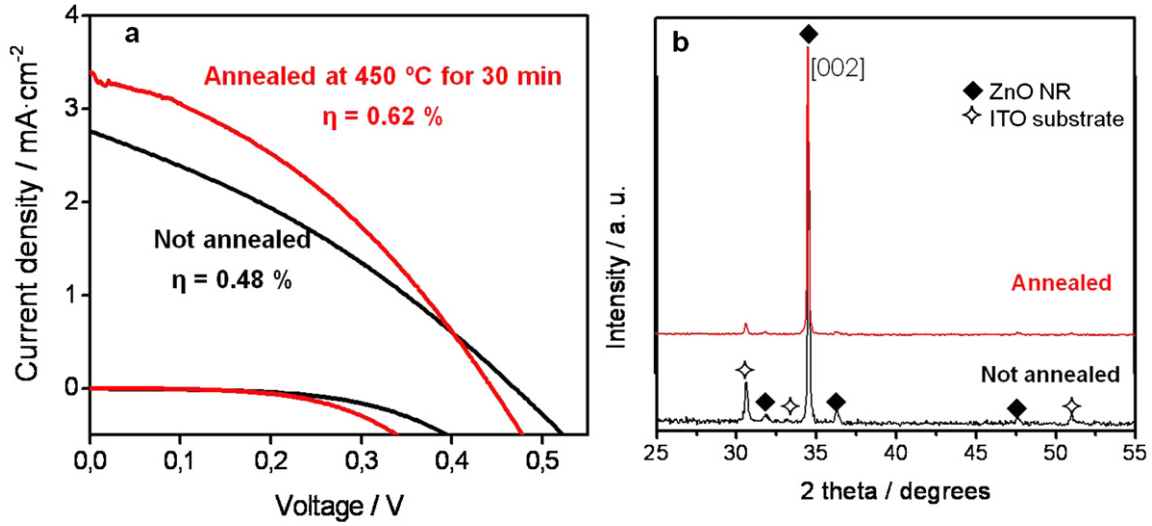

Fig. 7. Vertically-aligned electrode of ZnO, growth time 8 h, length ~2 μm. (a) *IV*-curve for the annealed and not annealed sample, dye loading 1 h, measured at 1000 W m^{-2} and (b) X-ray powder diffraction of the annealed and not annealed samples.

Table 1
Performance of DSCs made with vertically-aligned ZnO NRs (average of 5). Effect of the ZnO NRs growth time on solar cell efficiency. 1.5 A.M., 1000 W m^{-2}, no UV filter applied.

NR growth time (h)	NR length (m)	DLT (h)	V_{oc} (V)	J_{sc} (mA cm^{-2})	FF (%)	Efficiency (%)	Max Eff. (%)	Temp. (°C)
At start								
6	1.6 ± 0.2	2	0.492 ± 0.061	2.34 ± 0.45	44 ± 4	0.46 ± 0.07	0.53	72
12	3.2 ± 0.2	3	0.487 ± 0.025	4.98 ± 0.38	41 ± 1	0.73 ± 0.07	0.80	72
22	5.2 ± 0.2	6	0.541 ± 0.046	3.47 ± 0.24	44 ± 2	0.81 ± 0.05	0.86	72
At max								
6	1.6 ± 0.2	2	0.553 ± 0.038	2.26 ± 0.42	44 ± 4	0.56 ± 0.04	0.60	72
12	3.2 ± 0.2	3	0.557 ± 0.008	3.38 ± 0.45	41 ± 1	0.80 ± 0.11	0.91	72
22	5.2 ± 0.2	6	0.559 ± 0.038	3.83 ± 0.40	45 ± 1	0.96 ± 0.06	1.02	72

DLT, dye loading time.

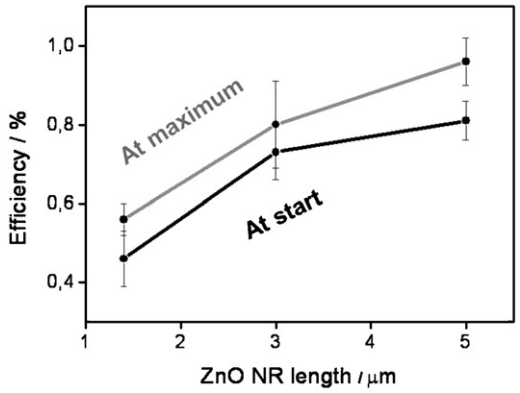

Fig. 8. Average performance of DSCs (of 5) made with vertically-aligned ZnO NRs. Effect of the ZnO NRs growth time on solar cell efficiency.

A series of ZnO NRs-based DSCs (up to 12) were analyzed. The photovoltaic properties of the solar cells (average of 5 samples) depending on ZnO nanorod length are detailed in Table 1. The power conversion efficiency was observed to increase when NR length increases up to 5.2 μm at 22 h growth time. We also observed a 10–15% improvement in power conversion efficiency after a few days after the initial DSC testing. The maximum value was observed after 3 days since DSC fabrication (keeping the devices in the dark at room temperature) (Fig. 8). We have previously attributed this enhancement to the effect that UV light shows on dye chemisorption in ZnO [24]. Table 1 shows detailed photovoltaic values and the improvement observed in solar cells performance after 3 days. The improvement has been observed to be due to the increase on V_{oc} after standing for 3 days in the dark. These changes in V_{oc} indicate the modification of the energy levels within the solar cell, probably due to the chemisorption of the dye into the ZnO as already reported [24]. Fig. 9 shows the best IV-curves and IPCE spectra obtained for these set of DSCs (obtained after 3 days stabilized in the dark).

Thus, as a summary, we report in this section on the best photovoltaic performance which was observed when (a) the ZnO NR electrodes are annealed at 450 °C for 30 min, (b) the dye loading time is optimized for each NR length between 10 min and 6 h and (c) when the DSC is stabilized for at least 3 days after fabrication.

3.3. Temperature, UV light and light intensity dependence

The effect of temperature, UV filter or light intensity has been analyzed by a few groups, mainly for TiO_2-based DSC, sometimes with contradictory results [33–37]. Parameters such as temperature are expected to affect diffusion and thus J_{sc} and efficiency of the final DSC. In TiO_2-based solar cells some authors have reported on the almost null effect of temperature when low levels of irradiation are applied [33]. Others demonstrated that values of V_{oc} are reduced when temperature increases [35]. Moreover, most DSCs are analyzed under 1 sun illumination, but a few reports show the effect of light intensity on DSC performance. In many cases variation of real temperature and light intensity is observed to be between −10 °C and 60 °C and from very low light irradiation (e.g. northern Europe) up to high irradiation levels, depending on the time of the day and the location. The study of these parameters permits the understanding of the DSC response under real (outdoor) conditions. Thus, in this section we report for the first time, a systematic study on the effect of temperature, UV light and light intensity on vertically-aligned ZnO NRs-based DSCs.

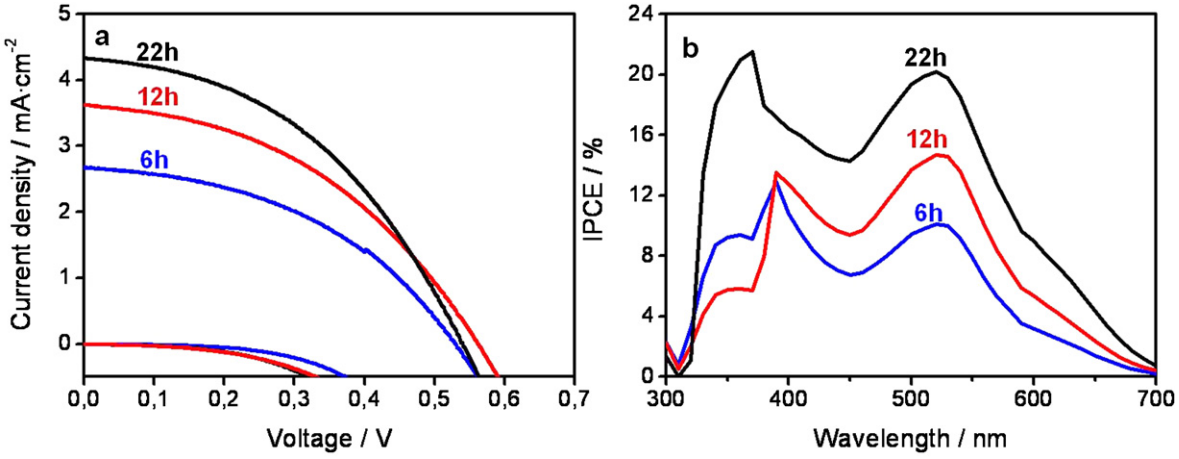

Fig. 9. (a) IV curves for DSCs with ZnO NRs grown at 6 h, 12 h and 22 h at maximum performance (after 3 days) and (b) IPCE spectra for the same cells. 100 mW cm^{-2} A.M. 1.5G. Active area 0.2 cm^2.

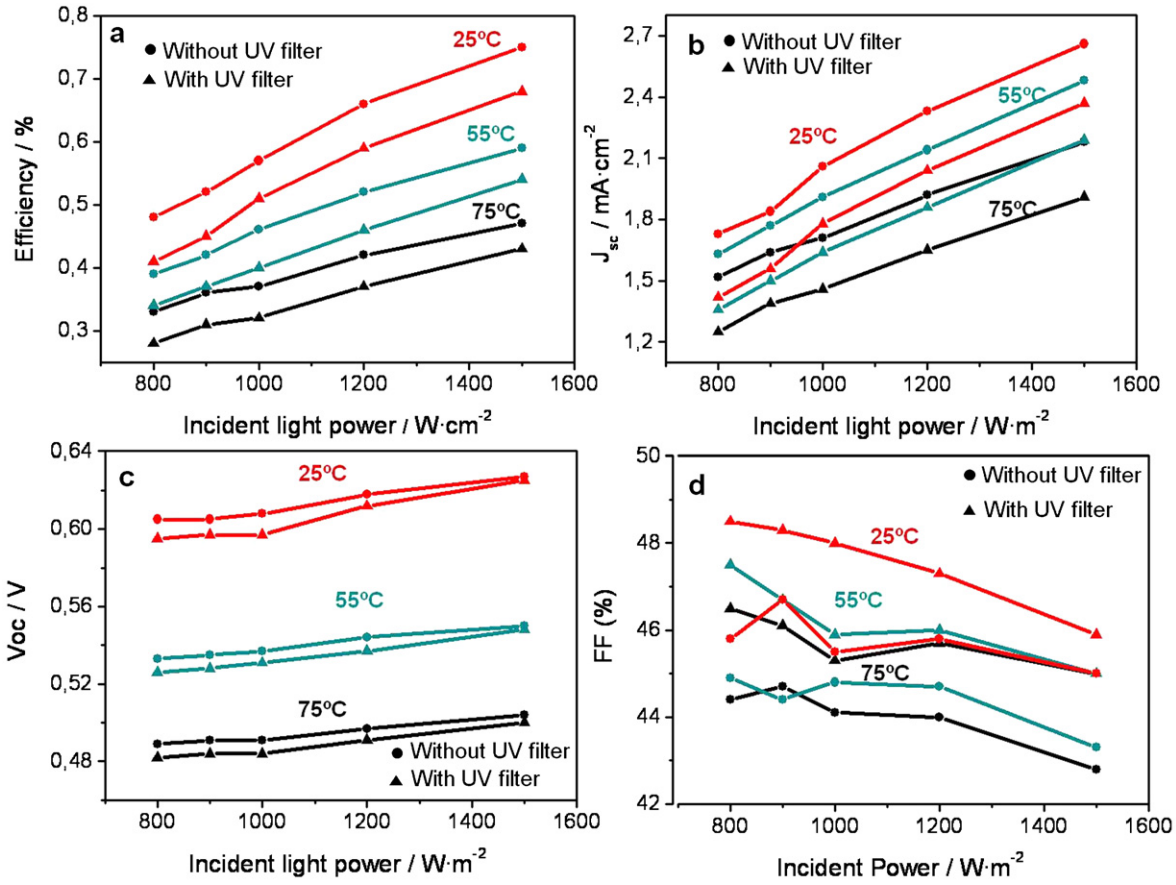

Fig. 10. Dependence of DSC parameters measured at different temperatures (25 °C, 55 °C and 75 °C) and at different light intensities (800–1800 W m^{-2}) with and without a UV–vis filter (<400 nm). (a) Efficiency, (b) J_{sc}, (c) V_{oc} and (d) FF. DSC made of vertically aligned ZnO NRs grown for 6 h (~1.8 μm) and 2 h sintered. N719 dye used. Active area was 0.2 cm^2.

3.3.1. *Effect of temperature*

Temperature is known to modify photovoltaic response of dye sensitized solar cells based on TiO_2, due to its effect on charge diffusion, thus temperature increase results in higher charge recombination [33–37]. In our ZnO-based DSC we observed a similar trend: photovoltaic response decreases when temperature is raised from 25 °C to 75 °C. Fig. 10 shows the changes observed on efficiency, V_{oc}, J_{sc}, and Fill Factor (FF) for the DSCs measured. The most drastic effect was observed in V_{oc}, which decreased from ~0.6 V down to ~0.48 V when temperature increases (Fig. 10c). A similar trend was observed for the short-circuit current (J_{sc}) that, until 55 °C, was maintained almost unchanged. Above 55 °C, the temperature affects negatively the J_{sc} as observed in Fig. 10b. The latter effect is attributed to the efficient electron diffusion observed in semiconductor oxides as temperature increases. Nevertheless, temperature promotes charge recombination which can reduce J_{sc} and V_{oc} and therefore the power conversion efficiency [33–37]. Since FF is directly related to V_{oc} and J_{sc}, it is not surprising to observe a variation of the FF between 2 and 3% depending on the temperature.

3.3.2. *Effect of the incident light intensity*

The dependence of light intensity and V_{oc} is a characteristic of excitonic solar cells [34–39], like TiO_2-based DSC [39] and also for polymer solar cells [38]. The increase of open-circuit voltage when light intensity increases has been attributed to the increase on charge generation rate. The latter provokes a larger chemical potential to build up within a DSC based on TiO_2 [39]. In the case of ZnO-based DSCs, the V_{oc} also increased when light intensity increased suggesting that a same response is taking place. Nevertheless, in our devices V_{oc} changes were observed to vary from 0.58 V up to 0.62 V when light intensity was modified from 800 W m^{-2} up to 1500 W m^{-2}. These values were lower at intensities below 1000 W m^{-2}, where V_{oc} was maintained almost unchanged. Only FF values were shown to decrease slightly with light intensity, with a variation between 2 and 3%.

3.3.3. *UV light*

The only difference between the application or not of a UV filter (Fig. 10a and b) is a variation in J_{sc}, which is slightly lower when an UV-filter is applied. The latter is not surprising, since about 5% of solar light correspond to UV light. Nevertheless, UV light is known to be destructive for TiO_2-based DSC since oxygen migrates from the semiconductor oxide photogenerating holes that accelerate the oxidation of the dye. In a ZnO-based DSC, a slightly dissimilar behaviour has been reported, which has also been observed in organic solar cells where the ZnO is applied as buffer layer. In the latter cases, UV light seems to promote the physisorption/chemisorption of organic molecules (polymers or dyes) [24] improving, at least initially, the photovoltaic performance of the solar cells. In the case of DSC, the chemisorption of the dye molecules on ZnO results in the formation of a [dye–Zn^{2+}] complex [24]. In organic solar cells, the extraction of oxygen from the ZnO after UV light irradiation seems to be the responsible of the increase of power conversion efficiency by the formation of a charge transfer complex between oxygen and the polymer [66]. Comparison of shunt resistance (R_{sh}) and series resistance (R_s) values for the DSCs analyzed in this work, with and without the presence of UV filter can give an insight on this effect. In principle, we search for low R_s values, which imply less parasitic loss, and high values

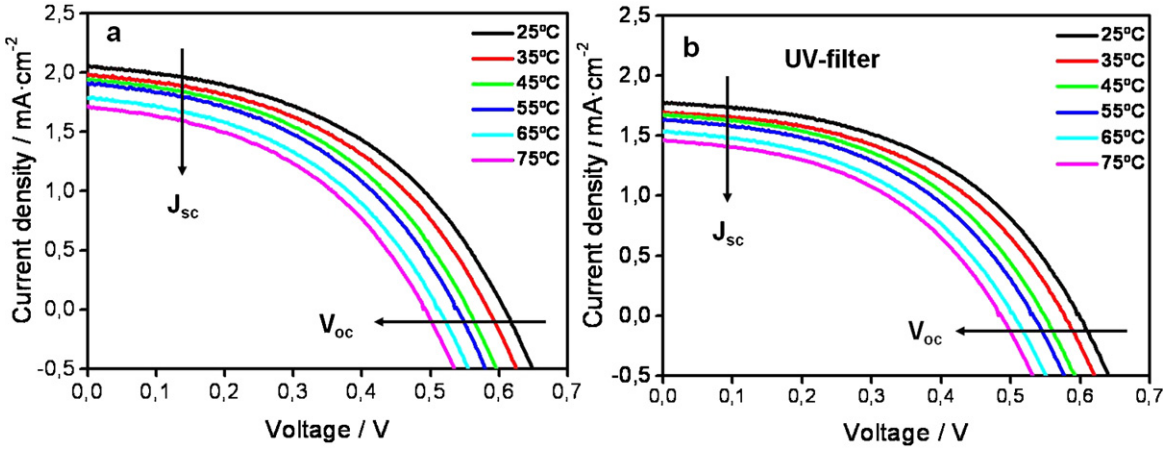

Fig. 11. IV curves for a DSC of 6 h ZnO NRs (~1.8 μm) and 2 h sintered with N719 dye. (a) DSC measured at different temperatures and (b) the same DSC measured using a UV filter (<400 nm) at different temperatures. 100 mW cm^{-2} A.M. 1.5G. Active area 0.2 cm^2.

Table 2
Solar cell parameters of a DSC at 100 mW cm^{-2} for different temperatures measured without and with a UV filter.

Temp (°C)	V_{oc} (V)	J_{sc} (mA cm^{-2})	FF	Eff (%)	R_{sh} (cm^2)	R_s (cm^2)
No UV-filter						
25	0.608	2.06	0.46	0.57	1957	89.9
35	0.583	1.98	0.46	0.53	1736	90.8
45	0.555	1.94	0.46	0.46	1707	90.2
55	0.537	1.91	0.45	0.46	1523	91.7
65	0.513	1.79	0.44	0.40	1754	95.5
75	0.491	1.71	0.44	0.37	1519	95.2
UV filter						
25	0.597	1.78	0.48	0.51	3651	96.0
35	0.577	1.70	0.47	0.46	2482	98.0
45	0.548	1.67	0.47	0.43	2689	97.5
55	0.531	1.64	0.46	0.40	2219	99.6
65	0.504	1.53	0.45	0.35	2716	104.3
75	0.484	1.46	0.45	0.32	2227	103.9

of R_{sh}, indicating low internal loss and less recombination. These requisites are needed in order to increase power conversion efficiency of our devices. Table 2 shows the R_s and R_{sh} values measured at 1000 W m^{-2} and at different temperatures with and without the application of UV-filter, values were obtained from IV curves shown in Fig. 11. Values of R_s are between 89 and 95 Ω cm^2 and 96–100 Ω cm^2 for solar cells without and with the application of UV filter, respectively. These values are considered very similar and are in well agreement with published results of ~140 Ω cm^2 for ZnO nanowires DSC (for 3.2 μm long) [40]. The presence or absence of UV light has shown considerable differences in R_{sh}. Without UV filter, R_{sh} values are between 1519 and 1957 Ω cm^2, with the highest values obtained at lower temperatures (see Table 2). The application of UV filter increases R_{sh} values to 2227–3651 Ω cm^2, as expected, the highest R_{sh} values are also observed for lower temperatures. These results indicate that recombination is reduced when eliminating the presence of UV light and when the devices are working at low temperatures [41,42].

IPCE analyses of the DSC showed three peaks, one at ~350 nm, a second one, no so evident, at ~380 nm and a third one at ~520 nm. The first peak ~350 nm corresponds to the ZnO and those at ~380 nm and ~520 nm have been attributed to the absorption of the dye. At different temperatures the intensity of the peaks at ~350 nm and ~380 nm decreases when the temperature increased. A different behaviour was observed for the peak at ~520 nm which remained constant until 55 °C but decreased when increased the temperature up to 75 °C. The latter is in well-correspondence with the J_{sc} behaviour observed before at different temperatures (see Fig. 12a). The evolution of the IPCE peaks with time shows the increase of the peak at 380 nm, while the peak at 520 nm decreases (Fig. 11b) [24], an indication of dye degradation.

3.4. Long-term analysis under continuous irradiation conditions

Long-term stability analyses of the DSC were carried out at 45 °C and 1000 W m^{-2}. We have reported that the interaction between

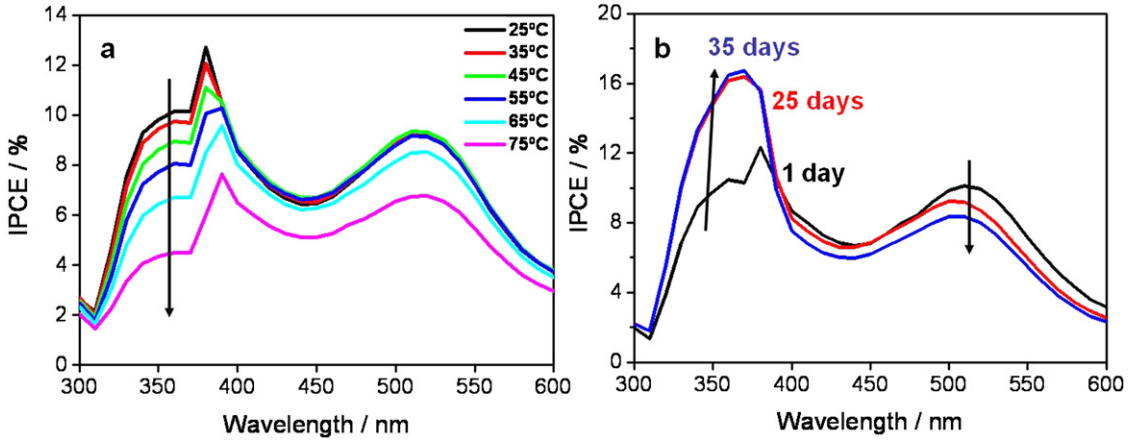

Fig. 12. IPCE spectra for a DSC of 6 h ZnO NRs (~1.8 μm) and 2 h sintered with N719 dye. Variation of IPCE with temperature (a) and time (b).

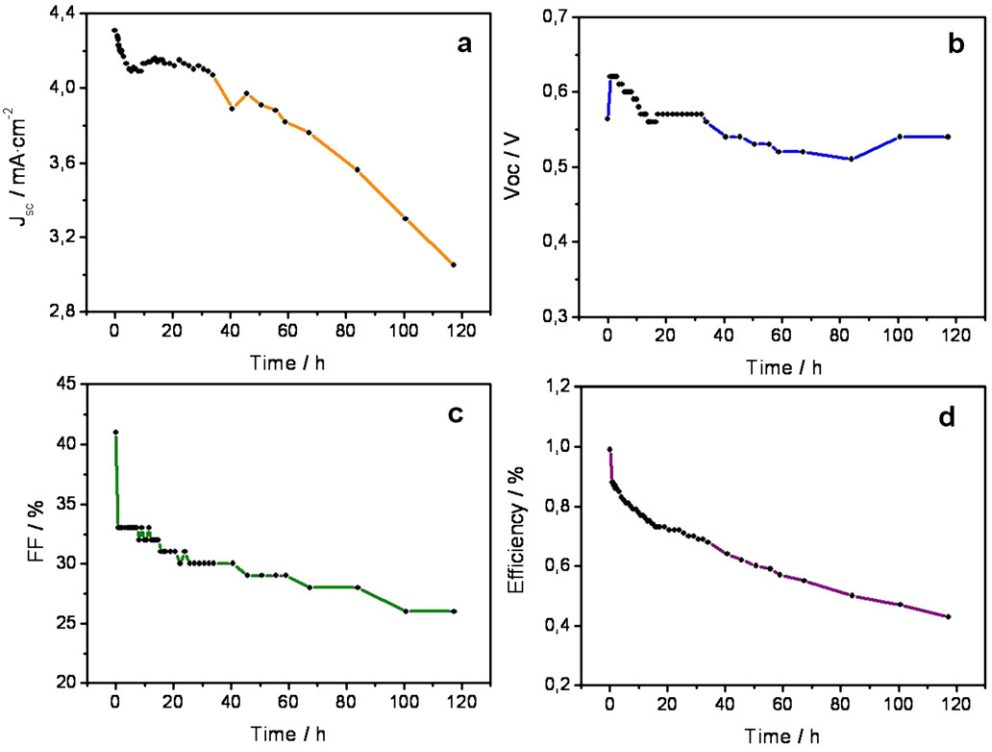

Fig. 13. Continuous irradiation experiment carried out at 100 mW cm^{-2} for a DSC with 5 μm ZnO NR. (a) J_{sc}, (b) V_{oc}, (c) FF and (d) power conversion efficiency. DSC made with vertically aligned ZnO NRs grown for 6 h.

the N-719 dye and the ZnO NRs seem to take place in 3 well-defined steps: dye diffusion, dye chemisorption and complex $[dye–ZnO]^{2+}$ formation [24]. UV-light irradiation permits a faster interaction between the dye and the ZnO but faster degradation of the cell is also observed. Without UV-light irradiation the latter process also takes place, but in a slower mode [24]. The latter was observed for a sample of 5 μm ZnO NR length analyzed under continuous irradiation at 1 sun. Fig. 13 shows the degradation process for all the parameters from the DSC. After 40 h of irradiation the J_{sc} shows a faster degradation but V_{oc} was almost constant during all the measurement (Fig. 13a and b). On the other hand, the efficiency of the cell decreased exponentially.

In order to study the latter effect, vertically-aligned ZnO NRs were scratched from an electrode and suspended in an ethanolic solution containing the dye N719, the mixture was stirred for 1 month. A pink solid was observed in the solution with time. The solid was centrifuged and washed with ethanol before analyses. TEM characterization of the solids in the solution showed a slight degradation of the ZnO NRs, the formation of a very thin core-shell organic layer covering all the NRs was observed (Fig. 14a and b). EDX analyses of the organic layer indicated the presence of Ru from the dye. The effect of the DSC electrolyte was also analyzed by adding some drops of electrolyte to the ethanol/dye/ZnO mixture. After analyses, small pieces of aggregates were observed all over the sample (Fig. 14c). Our results show that the dissolution of the dye is not only due to the interaction between the dye and the ZnO but also by the effect imposed by the electrolyte. Moreover, our results indicate a clear interplay between the dye, the electrolyte and the temperature. HR-SEM images of the aggregate (ZnO NRs + dye N719) are showed in Fig. 15. TGA analyses of the aggregate showed the presence of a highly hygroscopic solid, which weight loss was less than 1% (organic matter) below 550 °C.

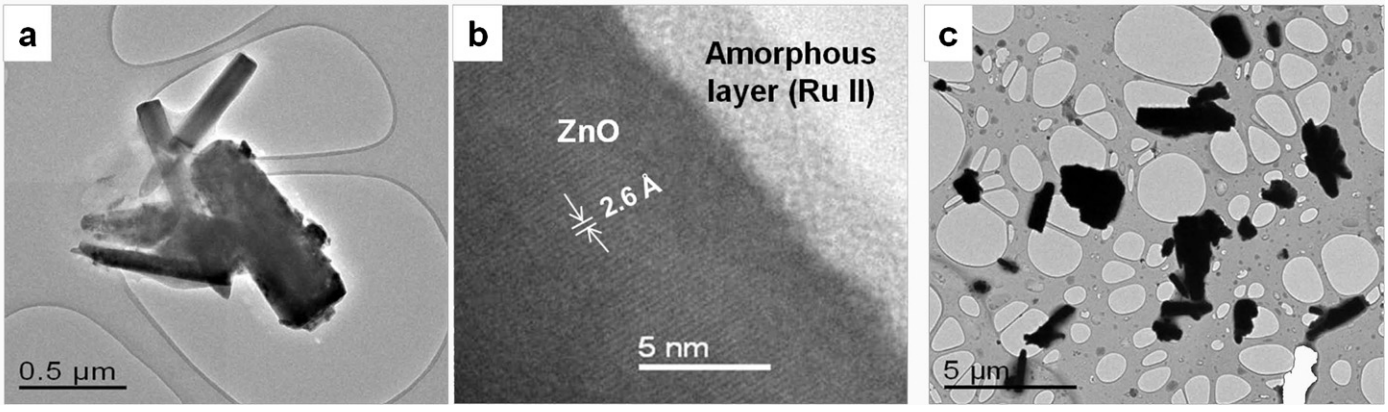

Fig. 14. FE-TEM images. (a) Solution of ZnO NRs and N719 dye. (b) High-magnification image of one ZnO NR from the solution (a) and (c) Solution of ZnO NRs with N719 dye and electrolyte.

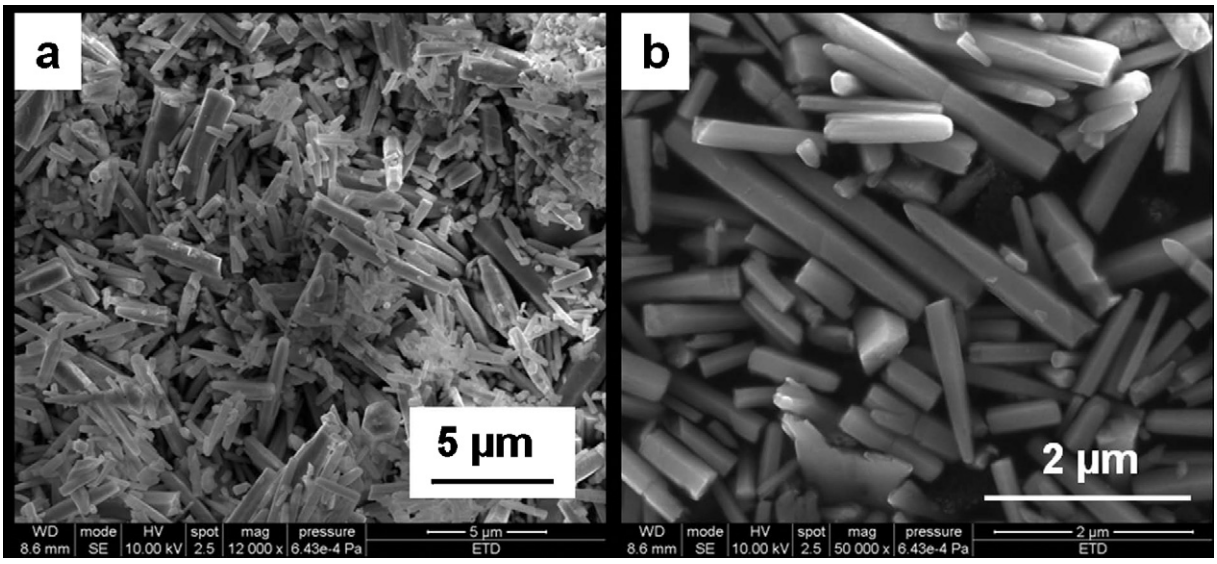

Fig. 15. HR-SEM images. (a) Big aggregates of ZnO NRs and N719 dye from the solution. (b) Higher magnification image of the solid.

4. Comparison with reported values

We have made an extensive review on the photovoltaic performance of vertically aligned ZnO NRs and their application in DSC [1]. Fig. 16 and Table 3 present an updated version, including 2009 and 2010 published works (squares), and the results obtained in our laboratory at CIN2 (red triangles/red line). (For interpretation of the references to color in text, the reader is referred to the web version of the article.) The data included corresponds to DSC taking into account only vertically-aligned ZnO NRs based DSCs. Works where the co-existence of other semiconductor oxide (such as TiO_2), or other nanoform is present (core–shell, nanoparticles decorated NRs, nanoflowers, etc.) have been excluded. Analyzing the bibliography, we have observed that most of the reported values refer to the hydrothermal synthesis (or chemical bath method) of the ZnO NRs, where the chemical synthesis of the NR is similar or the same as the one applied in this work. Only the data labelled as (c), from [44], in Fig. 16 refers to the growth of ZnO NRs by anodization of Zn, which we believe is the reason for the higher performance observed for this sample at ~3 μm NR length. Data labelled as (a), from [22], corresponds to the highest power conversion efficiency ever published for DSC applying the bare ZnO NRs (vertically aligned). Only recently, another group achieved a 2.3% efficiency, applying 1 μm NR length and a different electrolyte [43], data labelled as (b) in Table 3. A curious aspect in these 2 publications [22] and [43] is that both have very high values of J_{sc}, similar to J_{sc} obtained for ZnO NR with lengths of about 14–16 μm (Table 3). No reproducibility of this efficiency value has ever been reported again by any other laboratory.

Analyzing the reported values in Fig. 16 and Table 3 (and leaving aside data from a [22], b [43] and c [44]), we have observed that there seem to be two distinctive values of power conversion efficiency which in turn are closely related to the length of the NRs. For NRs below 9 μm, efficiencies are never higher than 1.0%. Increasing NR length between 10 μm and 40 μm, the power conversion efficiency values observed are around 1.5%, with the maximum power conversion efficiency of 2.3%. The 9 μm length limit depends on the growth length since this length can be obtained within a 24 h growth time or less. Although, ZnO NRs have been proved to show better electron transport properties than ZnO nanoparticles, and better electron mobility than TiO_2 (meaning lower charge recombination) [53,54], the reported values indicate that there is some kind of limitation on the ZnO itself. Probably one of the main problems is related to the synthesis technique employed, but in-deep studies are required in order to understand the latter. For example, we have observed that most of the synthesis methods

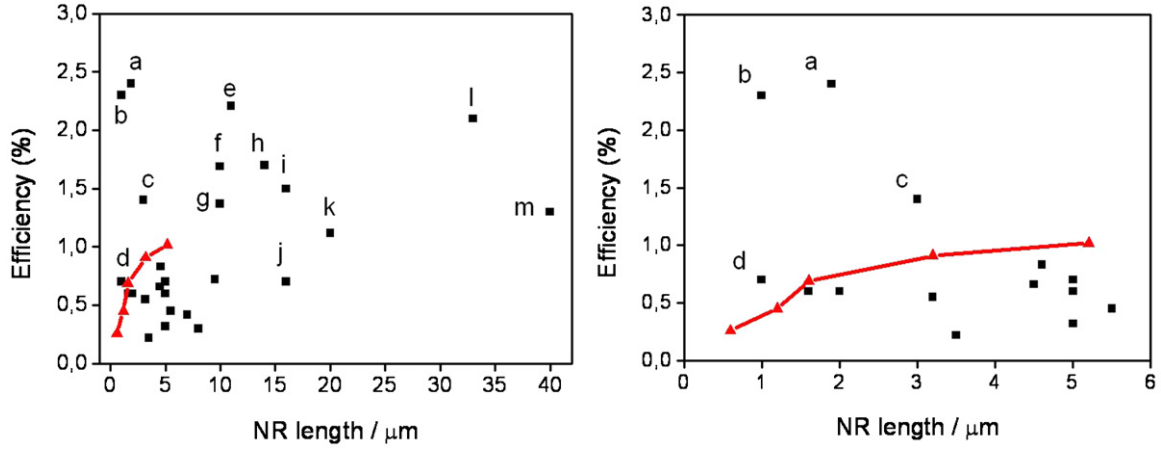

Fig. 16. Vertically-aligned ZnO NRs applied in DSC, comparisson between published data (squares) and values obtained at CIN2 (triangles) [24-this work]. The graph in the right is a closed look of curve on the left. References (a) [22], (b) [43] (c) [44], (d) [45], (e) [46], (f) [47], (g) [48], (h) [49], (i) [23], (j) [50], (k) [51], (l) [52] and (m) [14].

Table 3
Photovoltaic values published for DSC based on vertically-aligned ZnO Nanorods.

NR length (m)	Synthesis method	Dye	P_{max} (mW cm^{-2})	V_{oc} (V)	J_{sc} (mA cm^{-2})	FF (%)	Eff (%)	Ref
1.00	Hydrothermal/PEI	Z907	100	0.72	6.40	49.4	2.30	[43]
1.00	Hydrothermal	Rose Bengal	2	0.55	0.0490	55	0.70	[45]
1.60	Hydrothermal	N719	100	0.63	2.85	39	0.69	[24]
1.60	Hydrothermal	N719	100	0.53	2.67	41	0.60	This work
1.80	Hydrothermal	N719	–	0.47	4.79	32	0.71	[55]
1.90	Hydrothermal	N3	42	0.55	5.18	36	2.40	[22]
2.00	MOCVD	Porphyrin based	100	–	–	–	0.60	[56]
3.00	Zn anodization	N719	100	0.76	3.60	53	1.40	[44]
3.20	Hydrothermal	N719	100	0.56	3.62	41	0.91	This work
3.20	MOCVD	N719	100	0.66	2.04	41	0.55	[40]
3.50	Hydrothermal/CVD	N719	100	0.76	1.17	25	0.22	[57]
4.50	ECD	D149	100	0.60	3.28	33.3	0.66	[58]
4.60	Hydrothermal	Mercurochrome	100	0.51	3.30	48.9	0.83	[59]
5.00	Hydrothermal	N3	23.6	0.34	0.49	45	0.32	[60]
5.00	Hydrothermal	N719	100	0.50	3.80	30	0.70	[61]
5.00	CVD	N719	100	0.82	1.20	61	0.60	[62]
5.20	Hydrothermal	N719	100	0.60	3.72	45	1.02	This work
5.50	Hydrothermal	Mercurochrome	100	0.44	2.15	47	0.45	[63]
7.00	Hydrothermal	N719	100	0.55	1.50	40	0.42	[42]
8.00	Hydrothermal	N719	100	0.67	1.30	32	0.30	[41]
9.50	Hydrothermal	N719	100	0.54	2.25	59	0.72	[64]
10.0	Hydrothermal	N719	100	0.64	5.37	49	1.69	[47]
10.0	Hydrothermal	N719	100	0.65	5.51	38.2	1.37	[48]
11.0	Hydrothermal	N3	80	0.55	9.07	34	2.21	[46]
14.0	Hydrothermal	N719	100	0.54	6.79	50	1.70	[49]
16.0	Hydrothermal	N719	100	0.71	5.85	38	1.50	[23]
16.0	Hydrothermal	N719	100	0.76	1.84	47	0.70	[50]
20.0	Hydrothermal	N719	100	0.64	4.13	42.4	1.12	[51]
33.0	Hydrothermal	N719	100	0.67	9.30	34.1	2.10	[52]
40.0	Hydrothermal/PEI	N719	100	0.69	4.26	42	1.30	[14]

applied are the hydrothermal technique, CVD or Zn anodization. The data (c) in Fig. 16 shows higher power conversion efficiency in comparison to the DSCs with similar NR length. This data corresponds to the only DSC obtained with ZnO NRs synthesized by the anodization of Zn [44], indicating that the synthesis technique could be affecting the properties of ZnO and the final solar cell performance. In our current work, and in order to see the effect of the synthesis methodology, we have modified the synthesis technique described in this work. We have been able to increase power conversion efficiency of the solar cells applying ZnO NRs that are shorter than those reported here. The results prove that the crystalline structure and the mesoporosity of the ZnO NRs can be modified and that it plays a crucial role for photovoltaic performance. The latter work is currently part of a future publication.

5. Conclusions

We have synthesized vertically-aligned ZnO NRs and applied them as electrodes in DSC. The effect of different parameters during synthesis, have been demonstrated to play a crucial role on final photovoltaic properties. We present, for the first time, the analyses of different testing parameters affecting vertically-aligned ZnO-based DSC performance like light intensity, temperature and UV light. We have observed that increasing light intensity as well as temperature affect the series and shunt resistance of the devices reducing the final solar cell efficiency. Moreover, J_{sc} was observed to be affected by light intensity whereas V_{oc} is more directly related to temperature. Analysis of lifetime under continuous irradiation at 1 sun revealed the total dissolution of the ZnO NRs, with the consequent reduction on power conversion efficiency, after several hours. Comparison of the DSC performance of our devices with published data indicates that the synthesis technique applied could be behind the poor photovoltaic properties found for these ZnO-based DSC.

Acknowledgements

To the Spanish Ministry of Science and Innovation, MICINN, for the projects ENE2008-04373 (Nanostructured Materials for Organic and Dye Sensitized Solar Cells) and Consolider NANOSELECT CSD2007-00041, for the PhD scholarship awarded to I.G-V (BES-2009-028996) and the PTA-2008-1108-I contract to B.B. To the Spanish National Research Council, CSIC, for the PIE-200860I134 project (Synthesis and Characterization of Doped Oxides for Nanocrystalline Solar Cells) and the JAE-DOC contract awarded to Y.Y. To the Xarxa de Referència en Materials Avançats per a l'Energia, XaRMAE (Reference Center for Advanced Materials for Energy) of the Catalonia Government.

References

[1] I. Gonzalez-Valls, M. Lira-Cantu, Energy Environ. Sci. 2 (2009) 19–34.
[2] Y.-J. Lee, D.S. Ruby, D.W. Peters, B.B. McKenzie, J.W.P. Hsu, Nano Lett. 8 (2008) 1501–1505.
[3] J.Y. Chen, K.W. Sun, Solar Energy Mater. Solar Cells 94 (2010) 930–934.
[4] F.C. Krebs, S.A. Gevorgyan, J. Alstrup, J. Mater. Chem. 19 (2009) 5442–5451.
[5] F.C. Krebs, Solar Energy Mater. Solar Cells 92 (2008) 715–726.
[6] T. Shirakawa, T. Umeda, Y. Hashimoto, A. Fujii, K. Yoshino, J. Phys. D. Appl. Phys. 37 (2004) 847–850.
[7] C.-H. Hsieh, Y.-J. Cheng, P.-J. Li, C.-H. Chen, M. Dubosc, R.-M. Liang, C.-S. Hsu, J. Am. Chem. Soc. 132 (2010) 4887–4893.
[8] Q. Zhang, C.S. Dandeneau, S. Candelaria, D. Liu, B.B. Garcia, X. Zhou, Y.-H. Jeong, G. Cao, Chem. Mater. 22 (2010) 2427–2433.
[9] Q. Zhang, C.S. Dandeneau, X. Zhou, G. Cao, Adv. Mater. 21 (2009) 4087–4108.
[10] F. Zhao, J.-G. Zheng, X. Yang, X. Li, J. Wang, F. Zhao, K.S. Wong, C. Liang, M. Wu, Nanoscale 2 (2010) 1674–1683.
[11] V.V. Kislyuk, O.P. Dimitriev, J. Nanosci. Nanotechnol. 8 (2007) 1–18.
[12] Z.L. Wang, Mater. Today (2004) 26–33.
[13] Ü Özgür, Y.I. Alivov, C. Liu, A. Teke, M.A. Reshchikov, S. Dogan, V. Avrutin, S.-J. Cho, H. Morkoç, J. Appl. Phys. 98 (2005) 041301-103.
[14] J. Qiu, X. Li, F. Zhuge, X. Gan, X. Gao, W. He, S.-J. Park, H.-K. Kim, Y.-H. Hwang, Nanotechnology 21 (2010) 195602–195609.
[15] M. Lira-Cantu, F.C. Krebs, Solar Energy Mater. Solar Cells 90 (2006) 2076–2086.
[16] M.H. Aslan, A.Y. Oral, E. Mensur, A. Gül, E. Basaran, Solar Energy Mater. Solar Cells 82 (2004) 543–552.
[17] C. Pacholski, A. Kornowski, H. Weller, Angew. Chem. Int. Ed. 41 (2002) 1188–1191.

[18] T. Ma, M. Guo, M. Zhang, Y. Zhang, X. Wang, Nanotechnology 18 (2007) 035605–35607.
[19] L.E. Greene, M. Law, J. Goldberger, F. Kim, J.C. Johnson, Y. Zhang, R.J. Saykally, P. Yang, Angew. Chem. Int. Ed. 42 (2003) 3031–3034.
[20] L. Vayssieres, Adv. Mater. 15 (2003) 464–466.
[21] M. Ali, M. Winterer, Chem. Mater. 22 (2010) 85–91.
[22] M. Guo, P. Diao, X. Wang, S. Cai, J. Solid State Chem. 178 (2005) 3210–3215.
[23] M. Law, L.E. Greene, J.C. Johnson, R. Saykally, P. Yang, Nat. Mater. 4 (2005) 455–459.
[24] I. Gonzalez-Valls, M. Lira-Cantu, Energy Environ. Sci. 3 (2010) 789–795.
[25] M.K. Nowotny, L.R. Sheppard, T. Bak, J. Nowotny, J. Phys. Chem. C 112 (2008) 5275–5300.
[26] A. Moustaghfir, E. Tomasella, S. Ben Amor, M. Jacquet, J. Cellier, T. Sauvage, Surf. Coat. Technol. 174–175 (2003) 193–196.
[27] X.J. Wang, L.S. Vlasenko, S.J. Pearton, W.M. Chen, I.A. Buyanova, J. Phys. D Appl. Phys. 42 (2009) 175411–175418.
[28] D.C. Olson, S.E. Shaheen, R.T. Collins, D.S. Ginley, J. Phys. Chem. C 111 (2007) 16670–16678.
[29] X.Q. Wei, Z.G. Zhang, M. Liu, C.S. Chen, G. Sun, C.S. Xue, H.Z. Zhuang, B.Y. Man, Mater. Chem. Phys. 101 (2007) 285–290.
[30] M. Lira-Cantu, K. Norrman, J.W. Andreasen, F.C. Krebs, Chem. Mater. 18 (2006) 5684–5690.
[31] M. Lira-Cantu, M.K. Siddiki, D. Muñoz-Rojas, R. Amade, N.I. Gonzalez-Pech, Solar Energy Mater. Solar Cells 94 (2010) 1227–1234.
[32] M. Lira-Cantu, K. Norrman, J.W. Andreasen, N. Casañ-Pastor, F.C. Krebs, J. Electrochem. Soc. 154 (2007) B508–B513.
[33] H.J. Snaith, L. Schmidt-Mende, M. Grätzel, Phys. Rev. B 74 (2006) 045306.
[34] M. Toivola, L. Peltokorpi, J. Halme, P. Lund, Solar Energy Mater. Solar Cells 91 (2007) 1733–1742.
[35] M. Berginc, U. Opara Krasovec, M. Jankovec, M. Topic, Solar Energy Mater. Solar Cells 91 (2007) 821–828.
[36] L. Andrade, S.M. Zakeeruddin, M.K. Nazeeruddin, H. Aguilar-Ribeiro, A. Mendes, M. Grätzel, Chem. Phys. Chem. 10 (2009) 1117–1124.
[37] K. Ocakoglu, F. Yakuphanoglu, J.R. Durrant, S. Icli, Solar Energy Mater. Solar Cells 92 (2008) 1047–1053.
[38] J.A. Barker, C.M. Ramsdale, N.C. Greenham, Phys. Rev. B 67 (2003) 075205.
[39] T. Trupke, P. Würfel, I. Uhlendorf, J. Phys. Chem. B 104 (2000) 11484–11488.
[40] A. Du Pasquier, H. Chen, Y. Lu, Appl. Phys. Lett. 89 (2006) 253513.
[41] J.B. Baxter, A.M. Walker, K. van Ommering, E.S. Aydil, Nanotechnology 17 (2006) S304–S312.
[42] C.Y. Jiang, X.W. Sun, K.W. Tan, G.Q. Lo, A.K.K. Kyaw, D.L. Kwong, Appl. Phys. Lett. 92 (2008) 143101.
[43] Y. Xie, P. Joshi, S.B. Darling, Q. Chen, T. Zhang, D. Galipeau, Q. Qiao, J. Phys. Chem. C 114 (2010) 17880–17888.
[44] Z. Yang, T. Xu, Y. Ito, U. Welp, W.K. Kwok, J. Phys. Chem C 113 (2009) 20521–20526.
[45] B. Pradhan, S.K. Batabyal, A.J. Pal, Solar Energy Mater. Solar Cells 91 (2007) 769–773.
[46] R.S. Mane, W.-J. Lee, C.D. Lokhande, B.W. Cho, S.-H. Han, Curr. Appl. Phys. 8 (2008) 549–553.
[47] P. Charoensirithavorn, S. Yoshikawa, 2nd Int. Conf. on Sustainable Energy and Env. B-024, 2006, pp. 1–4.
[48] M.-H. Lai, A. Tubtimtae, M.-W. Lee, G.-J. Wang, Int. J. Photoenergy (2010) 1–5.
[49] Y. Gao, M. Nagai, T.-C. Chang, J.-J. Shyue, Cryst. Growth Des. 7 (2007) 2467–2471.
[50] A. Al-Hajry, A. Umar, Y.B. Hahn, D.H. Kim, Superlattices Mircrostruct 45 (2009) 529–534.
[51] J.X. Wang, C.M.L. Wu, W.S. Cheung, L.B. Luo, Z.B. He, G.D. Yuan, W.J. Zhang, C.S. Lee, S.T. Lee, J. Phys. Chem. C 114 (2010) 13157–13161.
[52] C.K. Xu, P. Shin, L.L. Cao, D. Gao, J. Phys. Chem. C 114 (2010) 125–129.
[53] M. Quintana, T. Edvinsson, A. Hagfeldt, G. Boschlo, J. Phys. Chem. C 111 (2007) 1035–1041.
[54] K. Keis, C. Bauer, G. Boschloo, A. Hagfeldt, K. Westermark, H. Rensmo, H. Siegbahn, J. Photochem. Photobiol. A 148 (2002) 57–64.
[55] J.Y. Chung, J.Y. Lee, S.W. Lim, Physica B 405 (2010) 2593–2598.
[56] E. Galoppini, J. Rochford, H. Chen, G. Saraf, Y. Lu, A. Hagfeldt, G. Boschloo, J. Phys. Chem. B 110 (2006) 16159–21616.
[57] Y.F. Hsu, Y.Y. Xi, A.B. Djurisic, W.K. Chan, Appl. Phys. Lett. 92 (2008) 133507.
[58] O. Lupan, V.M. Guerin, I.M. Tiginyanu, V.V. Ursaki, L. Chow, H. Heinrich, T. Pauporte, J. Photochem. Photobiol. A Chem. 211 (2010) 65–73.
[59] J.-J. Wu, G.-R. Chen, H.-H. Yang, C.-H. Ku, J.-Y. Lai, Appl. Phys. Lett. 90 (2007) 213109.
[60] H. Gao, G. Fang, M. Wang, N. Liu, L. Yuan, C. Li, L. Ai, J. Zhang, C. Zhou, S. Wu, X. Zha, Mater. Res. Bull. 43 (2008) 3345–3351.
[61] Z.H. Chen, Y.B. Tang, C.P. Liu, Y.H. Leung, G.D. Yuan, L.M. Chen, Y.Q. Wang, I. Bello, J.A. Zapien, W.J. Zhang, C.S. Lee, S.T. Lee, J. Phys. Chem. C 113 (2009) 13433–13437.
[62] A.-J. Cheng, Y. Tzeng, Y. Zhou, M. Park, T.-H. Wu, C. Shannon, D. Wang, W. Lee, Appl. Phys Lett. 92 (2008) 092113.
[63] C.-H. Ku, J.-J. Wu, Nanotechnology 18 (2007), 505706-9p.
[64] W.G. Yang, F.R. Wan, S.W. Chen, C.H. Jiang, Nanoscale Res. Lett. 4 (2009) 1486–1492.
[65] M. Lira-Cantu, A. Chafiq, J. Faissat, I. Gonzalez-Valls, Y. Youhai, Solar Energy Mater. Solar Cells 95 (2011) 1362–1374.
[66] M.R. Lilliedal, A.J. Medford, M.V. Madsen, K. Norrman, F.C. Krebs, Solar Energy Mater. Solar Cells 94 (2010) 2018–2031.